Fractional Charge by Fixed-Node Diffusion Monte Carlo Method

Matej Ditte[1] and Matúš Dubecký[1,2,*]
[1]Department of Physics, University of Ostrava, 30. dubna 22, 701 03 Ostrava, Czech Republic
[2]ATRI, Slovak University of Technology, J. Bottu 25, 917 24 Trnava, Slovakia

(Received 29 March 2019; published 9 October 2019)

Fixed-node diffusion Monte Carlo (FNDMC) method is a stochastic quantum many-body approach that has a great potential in electronic structure theory. We examine how FNDMC total energy $E(N)$ satisfies exact constraints, linearity and derivative discontinuity, versus fractional electron number N, if combined with mean-field trial wave functions that miss such features. H and Cl atoms with fractional charge reveal that FNDMC method is well able to restore the piecewise linearity of $E(N)$. The method uses ensemble and projector ingredients to achieve the correct charge localization. A water-solvated Cl^- complex illustrates superior performance of FNDMC method for charged noncovalent systems.

DOI: 10.1103/PhysRevLett.123.156402

Motivation.—Fixed-node diffusion Monte Carlo (FNDMC) method is a many-body stochastic quantum Monte Carlo (QMC) projector approach [1–4] that has been popular in electronic structure theory for its accuracy, scalability, and versatility [5–9]. FNDMC method acts in a continuum position space; for a Hamiltonian $\hat{H}$ it projects out an exact ground state (GS) Ψ that has nonzero overlap with the antisymmetric trial state Ψ_T, in imaginary time τ:

$$\Psi = \lim_{\tau\to\infty} \exp[-\tau(\hat{H} - E_T)]\Psi_T, \tag{1}$$

where E_T is an offset energy that keeps the norm of Ψ asymptotically constant. The total FNDMC energy is an upper bound to the exact energy [10] and the related FN bias goes quadratically with the nodal displacement error [4]. Ψ_T can be well sophisticated so that the related FN bias becomes negligible [11,12], nevertheless, practical FNDMC simulations feasible for large systems require simple and efficient *Ansätze* like the popular Slater-Jastrow wave function [13], $\Psi_T = \Psi_S J$, where Ψ_S is a single Slater determinant and J is a positive-definite explicit correlation Jastrow term [14].

Mean-field theories used to produce Ψ_S, including density functional theory (DFT) [15], as well as the states Ψ_S and Ψ_T (see below), however, miss fundamental constraints on exact electronic structure theory: the total energy $E(N)$ as a continuous function of a particle number N must show piecewise linear relationship with possible derivative discontinuities at integer N [16–18]. Lack thereof has been referred to as (de)localization error and it has severe consequences; it leads to an artificial charge adjustment and related spurious energy minimization which causes poor predictivity of charge-transfer, reaction barriers, band gaps, or noncovalent interactions (e.g., solvation of ions) [19,20]. In addition, $E(N)$ must also satisfy the constancy condition of fractional spin [18] important for correct description of strong correlation.

Here we examine how FNDMC method satisfies linearity of $E(N)$ for fractional N, and, derivative discontinuity at integer N, if combined with Ψ_T based on popular spin-restricted mean-field Ψ_S that show unphysical convex $E(N)$ dependency [20]. Such an analysis is important, for instance, to understand if the method is able to provide right energetics of charged noncovalent systems [19] for the right reasons. We consider atoms with fractional charge, H and Cl, to show that FNDMC method is well able to restore the piecewise linearity of $E(N)$ from the states that do not possess such a property. Walker population analyses indicate that the ensemble and projector features are both operative in this achievement. Insights gained from the water-solvated Cl^- complex suggest that accuracy and robustness of FNDMC simulations in charge-involving noncovalent interactions relate to the accurate charge localization.

Theory.—The effective fractional charge per atom was achieved for both H and Cl by modeling a cube (system) composed of 8 atoms (subsystems) of the same type separated enough so that the interactions between the subsystems can be neglected (infinite-separation limit). The Hamiltonian of such a system with $M = \sum_{i=1}^{8} N_i$ electrons,

$$\hat{H} = \sum_{i=1}^{8} \hat{H}^i, \tag{2}$$

satisfies the Schrödinger equation,

$$\hat{H}\Psi_k(M) = E(M)\Psi_k(M), \tag{3}$$

where

$$\Psi_k(M) = \hat{A}\left[\prod_{i=1}^{8} \Psi^i_{\alpha_i}(N_i)\right] \tag{4}$$

is a kth $g(M)$-times degenerate antisymmetric GS wave function $[g(M) = \prod_{i=1}^{8} g_i(N_i)]$ assembled as an antisymmetrized product of individual subsystem $g_i(N_i)$-times degenerate wave functions $\Psi^i_{\alpha_i}(N_i)$ that each satisfies

$$\hat{H}^i \Psi^i_{\alpha_i}(N_i) = E^i(N_i)\Psi^i_{\alpha_i}(N_i). \tag{5}$$

$\hat{A}$ is an M-electron antisymmetrization operator, and,

$$E(M) = \sum_{i=1}^{8} E^i(N_i) \tag{6}$$

is a corresponding degenerate total energy of the system. Addition of an integer charge q to such a system adds effective charge $q/8$ per subsystem thus enabling fractional charge as well.

QMC simulations of systems in a large separation limit require additional considerations for the lack of conventional VMC thermalization within usual simulation times (see Methods), and, nonergodicity [21–23] (electron localization on specific subsystems) due to the branching term in FNDMC simulations that eliminates configurations with small weights, including those with electrons possibly attempting to diffuse between the distant subsystems. Nevertheless, we argue that the total energy expectation values $\langle E \rangle$ from such FNDMC simulations are energetically correct.

In contrast to ergodic simulation where each walker would sample the mixed GS

$$\Psi(M) = \frac{1}{\sqrt{g(M)}} \sum_{k=1}^{g(M)} \Psi_k(M), \tag{7}$$

which is an eigenstate of $\hat{H}$ and leads to totally symmetric density, each walker $\mathbf{R}_j = (\mathbf{r}_1, \mathbf{r}_2, \mathbf{r}_3, \ldots, \mathbf{r}_N)_j$ in a properly initialized (from Ψ_T^2) nonergodic equilibrium FNDMC simulation randomly samples just one of the degenerate GS wave functions Ψ_k that generates symmetry-broken density and contributes to $\langle E \rangle$ according to the so-called mixed distribution $\Psi_k \Psi_T$ irrespective of its specific localization $\{N_i\}_j$ (i.e., a specific set of occupation numbers of the identical subsystems, labeled by i, here obtained by counting electrons in corresponding position-space octants). For Ψ_T that satisfy $\langle \Psi_T | \Psi_k \rangle \neq 0$ for all k, like, e.g., our Ψ_T based on a spin-restricted Slater determinant, it is not hard to accept that the population-based $\langle E \rangle$, of our sole interest here, is not affected by the walker localization and related density symmetry breaking.

Hydrogen cube.—First, we present the results obtained for the H_8 cube [20] with an edge of $a = 1000$ Å, 0–16 electrons, and singlet spin multiplicity ($N_\alpha = N_\beta$), allowing us to study essentially isolated H atom with an effective fractional charge in the range $0 \leq N \leq 2$, i.e., along the $H^+ \rightarrow H \rightarrow H^-$ pathway and $0.25e$ increments (Fig. 1). In agreement with the previous fractional-charge studies of H [18,20,24], we find that the considered mean-field methods, Hartree-Fock (HF) and DFT with the Perdew-Burke-Ernzerhof (PBE) [25] functional, miss linearity and the derivative discontinuity of $E(N)$ and show unphysical convex behavior instead (Fig. 1, red, blue). Interestingly, FNDMC simulations with related Ψ_T (cf. Fig. 3) recovered piecewise linear $E(N)$ dependency within the statistical resolution (Fig. 1, black). The results were indistinguishable for HF and PBE (more Ψ_T types were thus not considered). FNDMC simulation with Ψ_T based on PBE orbitals produced electron affinity EA(H)=0.713(1) eV to be compared vs the experimental value of 0.754 eV [26]. A slight discrepancy of ~0.04 eV is attributed to the use of the effective core potential (ECP) and residual FN bias due to 1-determinant [27]. Note that if the FNDMC method satisfies the linearity condition, the quality of the nodal surface determines only the slope of the actual $E(N)$ segment due to linearity-GS correspondence and the FNDMC projector nature (see below).

Chlorine cube.—Next we consider the Cl_8 cube ($a = 1000$ Å) in order to examine how FNDMC simulation describes fractional charge in a many-electron system. We consider only singlet states ($N_\alpha = N_\beta$). Effective fractional charge per Cl atom ranges between $16 \leq N \leq 18$ ($^1Cl^+ \rightarrow {}^2Cl \rightarrow {}^1Cl^-$) with $0.25e$ increments (Fig. 2). We observe that although the mean-field methods (HF, PBE, HSE06 [28]) miss linearity and derivative discontinuity [19] at point $N = 17$ per atom (neutral Cl), the FNDMC simulation well recovers both features from the related Ψ_T and produces accurate EA(Cl) = 3.64(2) eV consistent with experiment (3.613 eV [29]). It appears that FNDMC is well

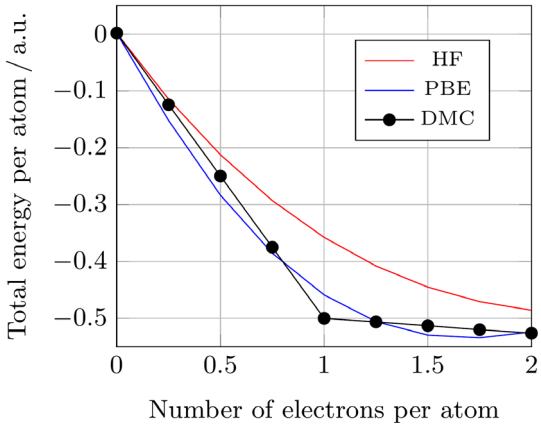

FIG. 1. Hydrogen cube: total energy $E(N)$ per atom vs electron occupation number N per atom obtained by mean-field (HF, PBE) and FNDMC (DMC) methods. FNDMC error bars (not shown) are smaller than the symbol size.

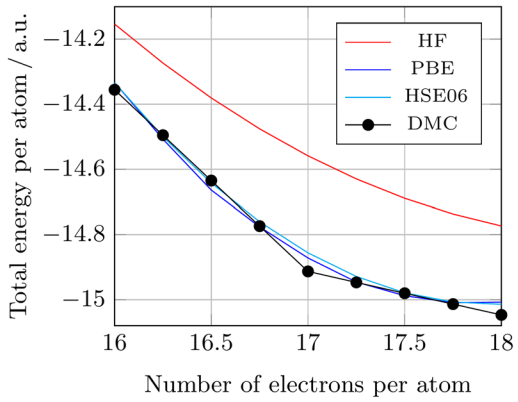

FIG. 2. Chlorine cube: total energy $E(N)$ per atom vs electron occupation number N per atom obtained by mean-field (HF, PBE, HSE06) and FNDMC (DMC) methods. FNDMC error bars (not shown) are smaller than the symbol size.

able to produce correct energetics in fractional-charge systems.

Wave function analysis.—Let us now focus on how FNDMC method achieves linearity of $E(N)$ in fractional charge models. As mentioned above, the electrons within each walker localize on specific centers, leading to the correspondence $\mathbf{R}_j \leftrightarrow \{N_i\}_j$ between the explicit (alive) walker position (varying along simulation) and subsystem occupation vector in occupation representation (fixed during the nonergodic simulation unless the walker dies out). Since each walker randomly samples just one of the degenerate GS wave functions Ψ_k, and the subsystem occupations randomly vary between the walkers, we find it convenient to introduce irreducible subsystem occupation vector $\vec{\lambda}_j$ obtained as a descending-ordered set of subsystem occupations $\{N_i\}_j$, $\vec{\lambda}_j = (\max\{N_i\}_j, \ldots, \min\{N_i\}_j)$. In addition, we introduce a corresponding vector of total subsystem spin momenta $\vec{\sigma}_j$ ordered in a descending way

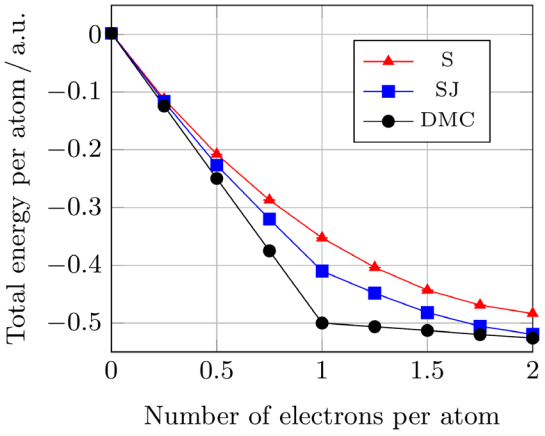

FIG. 3. Hydrogen cube: total energy $E(N)$ per atom vs electron number per atom from VMC with Ψ_S (S) and Slater-Jastrow Ψ_T (SJ) using PBE orbitals, and, FNDMC (DMC) simulation.

for each subset of identical λ_k. The pair $(\lambda_k, \sigma_k)_j$, labels the state of a subsystem k (after reordering) with λ_k electrons and a total spin momentum σ_k, as sampled by the walker j. We arrive at the more convenient correspondence, $\mathbf{R}_j \leftrightarrow |\vec{\lambda}, \vec{\sigma}\rangle_j$, that enables equal-footing comparisons between the walkers irrespective of the specific localization (and local position), and, unambiguous analysis of the system state within FNDMC simulation. We are interested in coefficients $\{c_{\vec{\lambda},\vec{\sigma}}\}$ of an expansion of irreducible GS,

$$\Psi(\mathbf{R}, \tau) = \sum_{\vec{\lambda},\vec{\sigma}} c_{\vec{\lambda},\vec{\sigma}} |\vec{\lambda}, \vec{\sigma}\rangle, \tag{8}$$

subject to $\sum_{\vec{\lambda},\vec{\sigma}} |c_{\vec{\lambda},\vec{\sigma}}|^2 = 1$, that could be obtained from a stochastic realization of $\Psi(\mathbf{R}, \tau)$ sampled by K walkers within equilibrium QMC simulation,

$$\Psi(\mathbf{R}, \tau) = \sum_{j=1}^{K} \delta[\mathbf{R} - \mathbf{R}_j(\tau)], \tag{9}$$

by virtue of the projectors,

$$\Psi(\mathbf{R}, \tau) = \sum_{\vec{\lambda},\vec{\sigma}} \sum_{j=1}^{K} |\vec{\lambda}, \vec{\sigma}\rangle \langle \vec{\lambda}, \vec{\sigma}| \delta_{\mathbf{R},\mathbf{R}_j(\tau)}\rangle. \tag{10}$$

For M electrons in the system with a specific partition $\vec{\lambda}_j$ between the subsystems, the GS consistent with the subsystem total energy convexity condition [16],

$$E^i(N) \leq \frac{1}{2}[E^i(N+1) + E^i(N-1)], \tag{11}$$

requires that each distant subsystem contains $a = \mathrm{int}(M/8)$ electrons, and, for nonzero $b = M - 8a$, b subsystems contain 1 additional electron each. We assume for the moment that $\vec{\sigma}$ is such that it minimizes the total energy and couples to the desired total spin momentum. For $M = 10$, any 2 of the 8 subsystems must contain 2 electrons and the remaining subsystems 1 electron each, $\vec{\lambda} = (2, 2, 1, 1, 1, 1, 1, 1)$, assuming a spin GS, e.g., $\vec{\sigma} = (0, 0, 0.5, 0.5, 0.5, -0.5, -0.5, -0.5)$ for a singlet H_8 cube. Other partitions $\vec{\lambda}$ (or non-GS $\vec{\sigma}$) represent excited-state configurations, e.g., $\vec{\lambda} = (2, 2, 2, 1, 1, 1, 1, 0)$, or, $\vec{\lambda} = (3, 1, 1, 1, 1, 1, 1, 1)$. Therefore, for the special case of distant identical subsystems, GS in the occupation-spin space may be conveniently identified by observing just 1-term in Eq. (8)-like expansions (note that this may not be an exact fermionic GS of $\hat{H}$ for the presence of fixed-node bias).

In Fig. 3, we compare the total energies $E(N)$ obtained for the H cube by VMC sampling of $|\Psi_S^2|$ and $|\Psi_T^2|$, and FNDMC simulation using Ψ_T. Clearly, contrary to the piecewise linear FNDMC total energy, the VMC total energies show

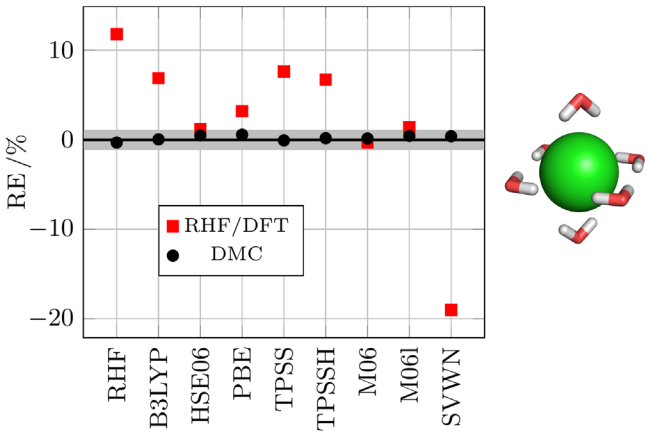

FIG. 4. Relatative errors (RE) of the interaction energies for the solvated anion $Cl^-(H_2O)_6$ complex (depicted) computed by RHF, DFT, and FNDMC simulations using Ψ_T based on the same orbitals, compared vs the CCSD(T)/CBS reference. Gray region indicates the benchmark level (1%). FNDMC error bars (not shown) are smaller than the symbol size.

convex behavior, although in the case of SJ, it seems that the derivative discontinuity starts to develop due to the partial excited-state suppresion by the Jastrow term [30–32] (examples follow in the next paragraph). For Ψ_S, the $E(N)$ curve is indeed consistent with the HF method reported in Fig. 1 within the statistical error.

Analysis of the related walker ensembles in terms of $|\vec{\lambda}, \vec{\sigma}\rangle$ configurations revealed multiconfiguration states containing large fractions of excited states for VMC, and, only GS configurations for FNDMC equilibrium ensembles, for all N, orbital types, and the Cl cube as well (cf. Fig. 5, Sec. I of the Supplemental Material [33]). For instance, PBE-based Ψ_S/Ψ_T of the neutral H cube with $N = 1$ electrons contained only 6%/11% of GS configurations and 6/5 types of configurations, whereas Ψ sampled by FNDMC simulation using Ψ_T contained GS configurations only. For $N = 1.25$, Ψ_S/Ψ_T contained 22%/38% of GS configurations and 6/4 configuration types, whereas, again, FNDMC ensemble contained 100% of GS. Details of such analyses for the H and Cl cubes, DFT and HF orbitals, VMC and FNDMC methods, and all considered N, are reported in Supplemental Material [33], Sec. IV.

The observation that FNDMC simulation produces 100% of GS configurations in our fractional-charge models is very important as it may improve our understanding of the method robustness in charged [34] and charge-transfer systems (e.g., reactions [35,36], excited states [37,38]). It has been shown [17] that the linearity of $E(N)$ for fractional N, and thus accurate charge localization, directly relates to the ability of a given method to produce only GS occupations. Namely, if the total energy of the system can be expressed [using identity $E^i(\lambda_i) = E^j(\lambda_i)$] as a linear combination of subsystem total energies,

$$E(M) = (8 - b)E^1(a) + bE^1(a + 1), \tag{12}$$

with a and b defined above and corresponding to the GS, then $E(N) = E(M)/8$ with $N = M/8$ is a piecewise linear function. That said, if an additional electron is put into a subsystem orbital in such a way that the GS of the system is maintained, then energy increments within a given segment of $E(N)$ are identical until the same-type orbitals are filled in all subsystems, which finishes a given (linear) segment. The success of FNDMC method in recovering the $E(N)$ piecewise linearity is thus attributed to the ensemble nature of the method causing that each electron resides on a specific subsystem at a time (fractional density is only possible via ensemble), and, projector property that apparently projects out proper (GS) configurations in charge-spin occupation space.

Application to $Cl^-(H_2O)_6$.—Finally, we consider a practical application of the concepts discussed above for noncovalent interactions of charged systems [34]. It was found that FNDMC simulation provides correct $E(N)$ dependency for the Cl cube contrary to the mean-field (Fig. 2). In systems with a charged Cl atom, one would thus generally expect that FNDMC results would be more robust than, say, DFT, and insensitive to the Ψ_T orbitals. We have considered interaction energies [9] (ΔE) of $Cl^-(H_2O)_6$ complex by various DFT approximations and FNDMC method using the same DFT functionals. Figure 4 summarizes the results and illustrates superior robustness of FNDMC simulations that reproduces the reference CCSD(T)/complete-basis-set results to within 1% for all Ψ_T. In contrast, ΔE from DFT and HF altogether varies by more than 20% due to the known (de)localization error, as revealed by the charge-population analysis (see Methods) detailed in Supplemental Material [33], Sec. III. Clearly, FNDMC simulations produce more robust and correctly more de- or localized charge population on Cl^- with respect to HF/DFT, respectively.

The qualitative difference between mean-field and FNDMC ΔE distributions is now easy to understand. Randomly chosen DFT determines fractional charge N from a certain interval according to its intrinsic delocalization error. In addition, it produces energy on a convex curve with its intrinsic curvature, that varies between functionals [39]. As a consequence, for a large set of DFT approximations, one obtains a large distribution of biases in the total energy of a complex, and, consequently, in ΔE, as observed. On the other hand, if FNDMC method predicts a correct charge localization, as expected from the results reported above, the fractional charge N in subsystems of a complex is accurate and more robust. Inaccuracy of Ψ_T dictates only the slope of the linear dependency (since the method always produces only GS charge-spin occupations), which leaves only a limited interval of bias that can be realized with varying (reasonable) Ψ_T. The dispersion of the results is thus much smaller, or, in other words, the method is much more robust, as observed, and we attribute its success to the accurate charge localization.

Summary.—Fractional-charge computations of H and Cl atoms revealed that FNDMC method is well able to restore the correct piecewise linear $E(N)$ behavior from Ψ_T that does not have such a property. Insights from the walker population analyses, in combination with formal discussions, indicate that FNDMC simulation correctly describes $E(N)$ linearity thanks to its ensemble nature and projection property. Inaccuracy of Ψ_T is expected to determine only the slope of $E(N)$ segments. This finding enables understanding of FNDMC robustness, as demonstrated in the noncovalent $Cl^-(H_2O)_6$ complex, from a new perspective. Study of fractional spin by FNDMC simulation is underway.

Methods.—Naive simulations of cube models with an edge of $a = 1000$ Å would not be straightforward because the conventional VMC equilibration times would vastly overcome the maximum simulation times available. In order to overcome this issue (without algorithm adjustments) in an automated fashion (avoiding manual initialization of configurations that may be biased by user imagination), the walkers for large-cube FNDMC simulations were initialized by ergodic VMC thermalization and stepwise quasiadiabatic extension of the system size starting from small a. We verified that the walker distributions produced in this way sample Ψ_T^2, and, in the case of a Slater determinant with HF orbitals, VMC reproduced the HF total energy for both H and Cl and all considered N. This was not the case for walkers initialized directly in a large cube. FNDMC computations used the QMCPACK [40] code with 16k target walker populations, imaginary time step of 0.005 a.u., and T moves [41]. Nuclei were represented by Burkatzki-Filippi-Dolg effective core potentials [42]. Single-determinant Slater-Jastrow Ψ_T were based on orbitals expanded in 1s-augmented valence triple-zeta (VTZ) one-particle basis sets without highest angular momentum channels [43] obtained with a tight SCF convergence (Gaussian G09 [44]). Jastrows containing up to electron-electron-nucleus terms, with a cutoff radius of 10 a.u., were optimized by the linear method [45], as usual, but cube simulations reused Jastrows optimized for H^- and Cl, respectively. The structure of $Cl^-(H_2O)_6$ (reported in the Supplemental Material, Sec. II [33]) was optimized at the MP2/aug-VTZ level (G09). The charge populations of the Cl atom in $Cl^-(H_2O)_6$ complex (Supplemental Material, Sec. IV [33]) were counted within a sphere around the Cl atom, with a radius $r = 2.033$ Å optimized to reproduce the CCSD natural charge, in order to obtain comparable population analysis. The used ensembles of walkers sampled Ψ_S with orbitals obtained from various functionals, and, the FNDMC mixed distribution. Approximately corrected "pure" charges were obtained via correction $\langle\Psi|\hat{O}|\Psi\rangle \approx 2\langle\Psi|\hat{O}|\Psi_T\rangle - \langle\Psi_T|\hat{O}|\Psi_T\rangle$ [46].

Fruitful discussions with Andrej Gendiar are gratefully acknowledged. We acknowledge financial support by the Czech Science Foundation (18-24321Y, 18-25128S), University of Ostrava (IRP201826), Slovak Research and Development Agency (APVV-18-0161) and, ERDF (ITMS 26220220179). The computations used IT4Innovations National Supercomputing Center (LM2015070).

*matus.dubecky@osu.cz

[1] J. B. Anderson, J. Chem. Phys. **63**, 1499 (1975).
[2] P. J. Reynolds, D. M. Ceperley, B. J. Alder, and W. A. Lester, Jr., J. Chem. Phys. **77**, 5593 (1982).
[3] C. J. Umrigar, M. P. Nightingale, and K. J. Runge, J. Chem. Phys. **99**, 2865 (1993).
[4] L. Mitas, E. L. Shirley, and D. M. Ceperley, J. Chem. Phys. **95**, 3467 (1991).
[5] J. Kolorenč and L. Mitas, Rep. Prog. Phys. **74**, 026502 (2011).
[6] A. Lüchow, WIREs Comput. Mol. Sci. **1**, 388 (2011).
[7] B. M. Austin, D. Y. Zubarev, and W. A. Lester, Chem. Rev. **112**, 263 (2012).
[8] M. A. Morales, R. Clay, C. Pierleoni, and D. M. Ceperley, Entropy **16**, 287 (2014).
[9] M. Dubecký, L. Mitas, and P. Jurečka, Chem. Rev. **116**, 5188 (2016).
[10] J. W. Moskowitz, K. E. Schmidt, M. A. Lee, and M. H. Kalos, J. Chem. Phys. **77**, 349 (1982).
[11] M. A. Morales, J. McMinis, B. K. Clark, J. Kim, and G. E. Scuseria, J. Chem. Theory Comput. **8**, 2181 (2012).
[12] R. Clay and M. A. Morales, J. Chem. Phys. **142**, 234103 (2015).
[13] D. Ceperley, G. V. Chester, and M. H. Kalos, Phys. Rev. B **16**, 3081 (1977).
[14] R. Jastrow, Phys. Rev. **98**, 1479 (1955).
[15] M. C. Per, K. A. Walker, and S. P. Russo, J. Chem. Theory Comput. **8**, 2255 (2012).
[16] J. P. Perdew, R. G. Parr, M. Levy, and J. L. Balduz, Jr., Phys. Rev. Lett. **49**, 1691 (1982).
[17] W. Yang, Y. Zhang, and P. W. Ayers, Phys. Rev. Lett. **84**, 5172 (2000).
[18] P. Mori-Sanchez, A. J. Cohen, and W. Yang, Phys. Rev. Lett. **102**, 066403 (2009).
[19] A. J. Cohen, P. Mori-Sanchez, and W. Yang, Science **321**, 792 (2008).
[20] P. Mori-Sánchez and A. J. Cohen, Phys. Chem. Chem. Phys. **16**, 14378 (2014).
[21] M. Casula, C. Filippi, and S. Sorella, Phys. Rev. Lett. **95**, 100201 (2005).
[22] M. Casula, S. Sorella, and G. Senatore, Phys. Rev. B **74**, 245427 (2006).
[23] L. Stella, C. Attaccalite, S. Sorella, and A. Rubio, Phys. Rev. B **84**, 245117 (2011).
[24] P. Mori-Sanchez and A. J. Cohen, J. Chem. Phys. **141**, 164124 (2014).
[25] J. P. Perdew, K. Burke, and M. Ernzerhof, Phys. Rev. Lett. **77**, 3865 (1996).
[26] K. R. Lykke, K. K. Murray, and W. C. Lineberger, Phys. Rev. A **43**, 6104 (1991).
[27] K. Gasperich, M. Deible, and K. D. Jordan, J. Chem. Phys. **147**, 074106 (2017).

[28] J. Heyd, G. Scuseria, and M. Ernzerhof, J. Chem. Phys. **124**, 219906 (2006).
[29] U. Berzinsh, M. Gustafsson, D. Hanstorp, A. Klinkmuller, U. Ljungblad, and A.-M. Martensson-Pendrill, Phys. Rev. A **51**, 231 (1995).
[30] M. C. Gutzwiller, Phys. Rev. Lett. **10**, 159 (1963).
[31] M. Capello, F. Becca, M. Fabrizio, S. Sorella, and E. Tosatti, Phys. Rev. Lett. **94**, 026406 (2005).
[32] B. Van der Goetz and E. Neuscamman, J. Chem. Theory Comput. **13**, 2035 (2017).
[33] See Supplemental Material at http://link.aps.org/supplemental/10.1103/PhysRevLett.123.156402 for comparison of Slater-Jastrow VMC vs FNDMC for Cl cube (analog of Fig. 3), xyz-structure and population analyses of the anionic water-solvated Cl^- complex, and, analyzes of walkers for H and Cl cube models from VMC and FNDMC simulations using various orbitals.
[34] V. Wineman-Fisher, Y. Al-Hamdani, I. Addou, A. Tkatchenko, and S. Varma., J. Chem. Theory Comput. **15**, 2444 (2019).
[35] E. T. Swann, M. L. Coote, A. S. Barnard, and M. C. Per, Int. J. Quantum Chem. **117**, e25361 (2017).
[36] K. Krongchon, B. Busemeyer, and L. K. Wagner, J. Chem. Phys. **146**, 124129 (2017).
[37] O. Valsson and C. Filippi, J. Chem. Theory Comput. **6**, 1275 (2010).
[38] M. Dubecký, R. Derian, L. Horváthová, M. Allan, and I. Štich, Phys. Chem. Chem. Phys. **13**, 20939 (2011).
[39] P. Mori-Sanchez, A. J. Cohen, and W. Yang, J. Chem. Phys. **125**, 201102 (2006).
[40] J. Kim *et al.*, J. Phys. Condens. Matter **30**, 195901 (2018).
[41] M. Casula, Phys. Rev. B **74**, 161102(R) (2006).
[42] M. Burkatzki, C. Filippi, and M. Dolg, J. Chem. Phys. **129**, 164115 (2008).
[43] M. Dubecký, J. Chem. Theory Comput. **13**, 3626 (2017).
[44] M. J. Frisch *et al.*, *Gaussian 09* (Gaussian, Inc., Wallingford CT, 2009).
[45] J. Toulouse and C. J. Umrigar, J. Chem. Phys. **126**, 084102 (2007).
[46] S. Guo, M. Bajdich, P. J. Reynolds, and L. Mitas, Mol. Phys. **111**, 1744 (2013).